AWARD NUMBER: W81XWH-18-1-0690, PC170350P2

TITLE: Therapeutic Targeting of Neuroendocrine Prostate Cancer

PRINCIPAL INVESTIGATOR: Eva Corey

CONTRACTING ORGANIZATION: University of Washington

REPORT DATE: SEPTEMBER 2021

TYPE OF REPORT: Annual

PREPARED FOR: U.S. Army Medical Research and Development Command
Fort Detrick, Maryland 21702-5012

DISTRIBUTION STATEMENT: Approved for Public Release;
Distribution Unlimited

REPORT DOCUMENTATION PAGE

Form Approved
OMB No. 0704-0188

1. REPORT DATE	2. REPORT TYPE	3. DATES COVERED
SEPTEMBER 2021	ANNUAL	9/1/2020-8/31/2021

4. TITLE AND SUBTITLE

Therapeutic Targeting of Neuroendocrine Prostate Cancer

5a. CONTRACT NUMBER
W81XWH-18-1-0690

5b. GRANT NUMBER
PC170350P2

5c. PROGRAM ELEMENT NUMBER

6. AUTHOR(S)
Eva Corey

E-Mail: ecorey@uw.edu

5d. PROJECT NUMBER

5e. TASK NUMBER

5f. WORK UNIT NUMBER

7. PERFORMING ORGANIZATION NAME(S) AND ADDRESS(ES)

University of Washington
4333 Brooklyn Ave
Seattle WA 98195-9472

8. PERFORMING ORGANIZATION REPORT NUMBER

9. SPONSORING / MONITORING AGENCY NAME(S) AND ADDRESS(ES)

U.S. Army Medical Research and Development Command
Fort Detrick, Maryland 21702-5012

10. SPONSOR/MONITOR'S ACRONYM(S)

11. SPONSOR/MONITOR'S REPORT NUMBER(S)

12. DISTRIBUTION / AVAILABILITY STATEMENT

Approved for Public Release; Distribution Unlimited

13. SUPPLEMENTARY NOTES

14. ABSTRACT

Neuronedocrine prostate cancer is an advanced form of this disease with very limited option of effective treatment. It has been shown that BRN2 is highly expressed in NEPC, and preliminary in vitro data show that inhibition of BRN2 decreases tumor cells growth. We will perform preclinical evaluation of efficacy of a novel BRN2 inhibitor alone, in combination with carboplatin (a standard therapy for neuroendocrine prostate cancer) to determine whether this treatment inhibits progression of NEPC and provides survival benefits.

15. SUBJECT TERMS

NONE LISTED

16. SECURITY CLASSIFICATION OF:			17. LIMITATION OF ABSTRACT	18. NUMBER OF PAGES	19a. NAME OF RESPONSIBLE PERSON
a. REPORT	b. ABSTRACT	c. THIS PAGE			USAMRMC
Unclassified	Unclassified	Unclassified	Unclassified	21	19b. TELEPHONE NUMBER *(include area code)*

TABLE OF CONTENTS

Introduction:

Prostate Cancer (PCa) is the most common male cancer and the 2nd leading cause of cancer deaths in North American men. While advanced PCa is initially controlled with hormonal therapies targeting the androgen receptor (AR) pathway, recurrence occurs due to emergence of lethal castration-resistant PCa (CRPC). Despite the potency of AR pathway inhibitors (ARPI) such us Enzalutamide (ENZ) that prolong survival, resistance ultimately emerges. Autopsy series suggest that up to 25% of CRPC patients resistant to ARPIs shed their dependence on the AR and exhibit a continuum of features associated with the neuroendocrine (NE) lineage (1). The diagnosis of Neuroendocrine Prostate Cancer (NEPC) is accompanied by a dismal overall survival measured in months, with decades old cytotoxic chemotherapy as standard treatment (2-4). Targeted treatments for this deadly disease are desperately needed. We were the first group to report that BRN2, a neuronal transcription factor, is sufficient and required to drive the evolution of an AR-driven adenocarcinoma into an aggressive and lethal AR-indifferent NEPC tumor (5). We have since developed a highly specific and potent small molecule BRN2 inhibitor (BRN2i). This project is centered on testing a new paradigm that epigenetic reprogramming, driven by BRN2, represents a molecular "conduit" to aggressive NEPC. In particular, how does BRN2 alter the architecture of the epigenome? Does BRN2 activate/regulate an intrinsic neurogenesis program? Can BRN2i prevent and/or treat NEPC?

To answer these questions, proposed a highly collaborative effort using innovative prostate cancer models coupled with state-of-the-art technologies, a series of ENZ-resistant (ENZR) including t-NEPC (5) and a large cohort of prostate cancer patient-derived xenografts. These established and novel PDX models serve as patient "avatars" that will ensure our research is relevant and rapidly translatable for treatment of aggressive prostate cancer, with immediate applications including; 1) deciphering the mechanisms underlying cellular plasticity leading to treatment resistance in PCa after hormone therapy; 2) exploring temporal changes in genetics/epigenetics during treatment-induced progression from adenocarcinoma to NEPC, and 3) testing therapeutic schemes, for example, when to best deploy BRN2i and whether they should be used as a monotherapy or in combination.

These studies will provide insight into how the epigenome is reprogrammed during the transition from an adenocarcinoma to NEPC in response to ARPIs by assessing fluxes in chromatin architecture and identifying the importance of BRN2 in mediating these processes. Our research posits that blocking that ability of cells to acquire a plastic phenotype via BRN2 inhibitor may delay/inhibit lineage transformation and extend the durability of clinically beneficial ARPIs and/or treat NEPC.

Key words

Prostate cancer, Neuroendocrine, Treatment, BRN2, small molecule inhibitor, ChIPseq, ATACseq, RIME

Accomplishments

1- Defining the molecular mechanisms by which BRN2 alters chromatin architecture to support neuroendocrine lineage reprogramming

We analyzed in depth BRN2 ChIPseq and started from a total of three sets of BRN2-bound genomic regions (BRN2 peaks) identified by ChIP-seq and MACS2 (logQ < -5) in one sample of $42D^{ENZR}$ cells and two replicate samples of NCI-H660 cells, a set of 5,454 reproducible NEPC BRN2 peaks (NEPC BRN2 Peak Set #1) was defined by finding all intersections of at least two of the three BRN2 peak sets (using bedtools) and removing any regions in the intersection that were < 10 bp. A more restricted set of 5,166 NEPC BRN2 peaks (NEPC BRN2 Peak Set #2) was obtained by removing any peaks in NEPC BRN2 Peak Set #1 that did not overlap any peak summits (located by MACS2) in the original three peak sets and subsequently replacing all remaining peaks by regions of fixed width (either 61 or 121 bp) centered on their average summit positions.

Additionally, to investigate whether NEPC might share a core set of BRN2-regulated elements with similar cancers of other tissues, BRN2 ChIP-seq peak sets (MACS2 logQ < -5) for two "neural" lung squamous cell carcinoma (nLUSC) cell lines (LK-2, 609 peaks; NCI-H520, 226 peaks) were downloaded from ChIP-Atlas, and a set of NEPC+nLUSC consensus BRN2 peaks was obtained by finding the intersection of NEPC BRN2 Peak Set #1 with the union of the two nLUSC peak sets, excluding any regions of intersection < 10 bp. This NEPC+nLUSC BRN2 consensus peak set contained 384 peaks, which overlapped 384/609 (63%) BRN2 peaks in LK-2 and 133/226 (59%) BRN2 peaks in NCI-H520. The high degree of overlap of BRN2 peaks between NEPC and nLUSC cell lines relative to the small numbers of peaks in the nLUSC cell lines suggests that the 384 NEPC+nLUSC consensus BRN2 peaks might represent a core set of BRN2-regulated elements that contribute to lineage infidelity of cancers across tissues. A list of potential target genes of the 384 core BRN2 peaks was generated using the genomic annotation tool UROPA to assign genes to peaks as follows: genes were assigned to a peak if either (1) they were within 1 kb of the peak or (2) the peak overlapped an enhancer with known links to the genes in any cell type according to the EnhancerAtlas 2.0 database. Enrichr analysis for gene sets (from the "ENCODE and ChEA consensus TFs from ChIP-X" library) over-represented in the list of potential BRN2 target genes revealed very strong enrichment for target genes of the transcription factor ZBTB33 (also known as Kaiso; $p = 1.7 \times 10^{-248}$, adjusted $p = 1.8 \times 10^{-246}$, odds ratio = 17.70). Similar Enrichr analysis following UROPA annotation (but excluding enhancers in order to limit the number of genes) of the broader NEPC BRN2 Peak Set #2 also indicated enrichment of Kaiso target genes among the genes within 1 kb of NEPC BRN2 peaks ($p = 7.5 \times 10^{-87}$, adjusted $p = 7.8 \times 10^{-85}$, odds ratio = 4.74). These results suggest that BRN2 may interplay with Kaiso to regulate transcription of genes.

To identify potential BRN2 cofactors in NEPC, ChIP-Atlas Enrichment Analysis was performed to identify peak sets (MACS2 logQ < -10) from individual ChIP-seq experiments (in any cell type) in the ChIP-Atlas database that significantly overlapped NEPC BRN2 Peak Set #2. Over 70% of the NEPC BRN2 peaks were found to overlap ChIP-seq peaks for Myc-associated factor X (MAX) in the context of small-cell lung cancer (SCLC) cell lines (NCI-H2171 and NCI-H128), and NEPC BRN2 peaks were also enriched for overlap with peaks from ChIP-seq experiments (in various cell types) for c-Myc, N-Myc, and Myc-associated zinc finger protein (MAZ) (**Figure 1a)** suggesting a possible relationship between BRN2 and the Myc/MAX network. More generally, proteins with a basic helix-loop-helix (bHLH) domain (which include MAX, c-Myc, and N-Myc) were enriched in this analysis (Enrichr, "HLH basic" gene set from the "Pfam Interpro Domains" library; **Figure 1a**). Additionally, NEPC BRN2 peaks were highly enriched for overlap with peaks from multiple BRD4 ChIP-seq experiments, including in neural cells, and with E2F1 ChIP-seq peaks, including in LNCaP cells (**Figure 1a**).

Enrichr analysis of the top antigens from the ChIP-Atlas Enrichment Analysis (logQ < -100, fold enrichment vs random > 10, overlaps > 10% of NEPC BRN2 peaks) indicated enrichment for members of the "G2-M Checkpoint" MsigDB Hallmark gene set among the antigens having greatest overlap of ChIP-seq peaks with NEPC BRN2 peaks, suggesting that potential cofactors of BRN2 may play a role in regulating the cell cycle (**Figure 1a**).

Restricting the ChIP-Atlas Enrichment Analysis results to only those interacting proteins that were specifically and reproducibly found by RIME to interact with BRN2 in both $42D^{ENZR}$ and NCI-H660 (proteins pulled down by BRN2 IP but not the corresponding IgG control IP in ≥ 2/3 42D replicates and 2/2 NCI-H660 replicates), the top results were highly enriched for factors involved in chromatin remodeling **(Figure 1b),** including multiple members of the NuRD and **SWI/SNF complexes** as well as related complexes (e.g. SNF2h-cohesin-NuRD), suggesting that BRN2 is involved in chromatin remodeling via interaction with these complexes. Interestingly, the top ChIP-Atlas results shared with RIME also included TP53BP1, which regulates p53 transcriptional activity and which separately functions in DNA double-strand break repair (Schultz et al., 2000, Cuella-Martin et al., 2016), and USP7, which stabilizes TP53BP1 via deubiquitination to regulate centrosome positioning (Kim and Yim, 2018, Yim et al., 2017). The NuRD complex has also been found to have a role in DNA damage repair (Smeenk et al., 2010) and to regulate p53 activity via deacetylation (Luo et al., 2000). Thus, these results together suggest that BRN2 may function in DNA damage repair, regulation of tumour suppressor p53, and mitotic chromosome organization. Other top hits in the ChIP-Atlas and RIME analysis included RBM25, HNRNPLL, and NCBP1, which all have functions in pre-mRNA splicing. Hence, BRN2 may be directly involved in regulation of pre-mRNA splicing in addition to regulating transcriptional expression of spliceosome.

Repeating the ChIP-Atlas Enrichment Analysis for only the 384 core BRN2 peaks shared between NEPC and nLUSC revealed that these shared peaks were strongly enriched for overlap with regions bound by Kaiso (ZBTB33; > 99% overlap of core NEPC+nLUSC BRN2 peaks; **Figure 2a)** in numerous cell types. This confirmed the earlier Enrichr analysis showing that Kaiso target genes were enriched among the list of potential BRN2 target genes. Curiously, however, Kaiso was absent from the list of reproducible BRN2 interactors identified by RIME in either 42D or NCI-H660, though Kaiso was identified as a BRN2 interactor in a recent third RIME replicate for NCI-H660 (experiment performed after completion of the ChIP-Atlas analysis described here). When restricted to the highly specific and reproducible BRN2 interactors identified by RIME in both 42D and NCI-H660, as described above, the analysis yielded similar results to those obtained for NEPC BRN2 Peak Set #2 (**Figure 2b–c**). Furthermore, Enrichr analysis showed that gene sets (from the "Reactome 2016" library) related to the cell cycle, chromatin organization and modification, and regulation of p53 activity were all significantly enriched among the most significant BRN2 interactors in the ChIP-Atlas results for the 384 core BRN2 peaks (**Figure 2c**). This further supports the possibilities laid out above that, in NEPC, BRN2 functions in chromatin remodelling, cell cycle regulation, and regulation of p53 activity. It also seems highly likely that there is interplay between BRN2 and Kaiso in regulating gene transcription, but this interplay could be a case of mutual exclusivity between the two factors. Together, the key findings of this analysis lend themselves to the following:

- BRN2 regulates chromatin organization/remodeling, pre-mRNA splicing, and cell cycle progression through direct interactions with important factors involved in these processes and also through transcriptional regulation of the expression of such factors
- BRN2 has functions in DNA damage repair and possibly in the regulation of TP53 activity.

2- Insight on BRN2-SWI/SNF complex:

We conducted rapid immunoprecipitation and mass spectrometry (RIME) to identify BRN2 interacting partners that help enable this function (Figure 3A). The experiment (validate by co-IP) revealed that in 42D^{ENZR} and NCI-H660, the BRN2 interacts with the Switch/Sucrose Nonfermenting (SWI/SNF) chromatin-remodeling complex (Figure 3B-C).

The BAF complex interacting with BRN2 includes the npBAF specific subunit, BAF53A (Figure 4A), a protein significantly upregulated in NEPC patients (Figure 4C). In addition to core subunits ARID1A, SMARCB1 and SMARCC1/2, BRN2 preferentially binds to BAF complex containing SMARCA4 and not SMARCA2 both in de novo and tNEPC models **(Figure 4B)** which is consistent with the increased SMARCA4 and decreased SMARA2 in NEPC (Figure 4D). Loss of SWI/SNF complex subunits create dependencies and further loss of function within the same complex leads to synthetic lethality. Analogous to the BRN2/npBAF complex, disruption of the Myc/cBAF complex through inhibition of MAX and SMARCA4 is synthetically lethal in small cell lung cancer. We next validated the RIME data and found that BRN2 binds to the core SWI/SNF subunits including SMARCA4 (BRG1), SMARCB1 (SNF5) and ARID1A (Figure 4E).

3- Effect of BRN2i on cell proliferation, apoptosis and NE in vivo

We performed an in vivo study using our novel BRN2 inhibitor (B18-94) in treatment-induced NEPC (42D^{ENZR}) and de novo NEPC (NCI-H660). We found that 50 mg/kg dose significantly reduces tumor volume in both 42D^{ENZR} and NCI-H660 models **(Figure 5A)**. Immunohistochemistry on end-of-study tumors demonstrated clear reduction in BRN2, SOX2 and Ki67 (cell proliferation) as well as an increase in CASP3 (apoptosis) **(Figure 5B)**. Additionally, B18-94 treated tumors had significantly reduced transcript levels of BRN2, SOX2, ASCL1 and PEG10 in both tumor models **(Figure 4C)**. Lastly, using the NCI-H660 model, we next compared the efficacy of B18-94 to standard of care platinum-based chemotherapy.

4- ***Effects of BRNi on PDX and analysis of the treated tumors***

The extend our cell line xenografts data, we evaluated effecst fo BRn2i in patiene-derived xenograft (PDX) models as described in the SOW. For the patient-derived xenograft (PDX) experiments, we identified BRN2 (POU3F2)-positive and negative neuroendocrine lines by RNAseq (**Figure 6**), immunohistochemistry (**Figure 7**), Western blot analysis (**Figure 8A**), and qPCR (**Figure 8B**). The first two PDX lines studied in year 2 of the project were LuCaP 93 (high expressor) and LuCaP 145.2 (little to no expression). We did not observe any significant change in tumor volume in either LuCaP 93 or LuCaP 145.2 after treatment with the BRN2i (**Figure 9**). To confirm BRN2 expression in both tumor types and to determine if BRN2 expression was altered after BRN2i treatment, we assessed all study tumors for BRN2 expression by IHC. As expected LuCaP 93 was positive for BRN2 (**Figure 10**) whereas LuCaP 145.2 was not. We did not observe any significant difference in BRN2 expression in tumors from treated compared to untreated animals (LuCaP 93 p=0.18).

We observed toxicity of the BRN2i in these first two PDX studies at UW, and had to decrease the dose, which potentially might be the reason why we observed no effects of the BRN2i in BRN2 positive LuCaP 93. In addition, for LuCaP studies we used CB17 SCID mice, a different mouse strain from the xenograft studies in UBC. The possibility was that the toxicity was related to the specific batch of the inhibitor used or mice strain. Therefore, we prepared a new batch of the inhibitor and tested its toxicity in CB17 SCID mice with increasing dose from 30 to 50 to 75 up to 100 mg/kg. In this experiment, all the doses were well tolerated in SCID mice. Thus, we proceeded and ran two additional studies using NEPC PDX LuCaP 49 and LuCaP 173.1, using the BRN2i that did not show toxicity and dosed at 50 mg/kg. Unfortunately, even with the new BRN2i, in both of these LuCaP PDX studies, we did not observe any significant anti-tumor activity (**Figure 9**). As in the previous two PDX studies, we confirmed that BRN2 was expressed

in the LuCaP 49 and 173.1 study tumors by IHC. Unfortunately, we again did not observe any significant difference in BRN2 expression when comparing BRN2i treated and untreated tumors (LuCaP 173.1 p=0.55; LuCaP 49 p=0.76).

To address the difference in efficacy in cell line xenografts and PDX studies, we performed RNASeq on the resulting tumors (RNAseq was performed on three independent PDX tumors from each arm of each study). As expected, POU3F2 was expressed in LuCaP 49, 93, and 173.1 by RNAseq. We then went on to evaluate genes of interest that were altered by BRN2i treatment in the responsive NCIH660 and 42D xenografts and non-responsive LuCaP 49, 93, and 173.1 xenograft tumors. We did not observe the differential expression of any genes with an FDR < 0.05 in the non-responsive lines; however, there was a significant number of genes that had an FDR < 0.05 in the responsive lines (**Figure 11**). To further explore the impact of BRN2i on the LuCaP xenografts, we performed a gene set enrichment analysis (GSEA) on the RNAseq data. Using a hallmark profile, it was very clear that hypoxia and inflammation pathways were significantly increased in the responsive xenograft tumors and proliferation-associated pathways were significantly decreased (**Figure 11A**). Whereas, no significant changes were observed in the non-responsive PDX tumors. This was even more apparent when we looked at individual lines in **Figure 11B**. To address the lack of observed activity in PDX models, we have designed a new more potent BRN2 inhibitor that we are currently evaluating *in vitro* and will proceed with *in vivo* evaluation during the no-cost extension.
Finally, to determine the impact of combined BRN2i and carboplatin treatment on gene expression profiles, we assessed NCIH660 tumors treated with vehicle control, BRN2i, carboplatin, or BRN2i+carboplatin by RNAseq. The GSEA showed an interesting phenomenon, where BRN2i decreased activity of the MYC and oxidative phosphorylation pathways, carboplatin significantly increased the activity of these two pathways (**Figure 11C**). We are currently exploring biological significance of these results for the use of BRN2i and carboplatin combination treatment of tumors *in vivo*.

Conclusion:

We used unbiased approach to delineate the mechanism of BRN2 by integrating our own ChIPseq and RIME with publicly available data in small lung cancer. We used a sophisticated bio-informatic analysis and discovered that BRN2 can communicate with the epigenome via its interaction with the SWI/SNF complex. More importantly, we found that BRN2 and a preference toward BAF complex and validated the finding by co-immunoprecipitation. We also presented the activity of BRN2 first in field small molecule inhibitor (B18-94) that significantly reduces tumor growth in multiple xenograft models, induces apoptosis and reduces cell proliferation and decreases BRN2 gene dependent in vivo. Overall, these data provide crucial proof-of-concept for targeting BRN2 in NEPC and open avenues for further investigation into other small cell tumor types. Unfortunately, as of now, our PDX preclinical testing did not provide results indicating BRN2i inhibitory effects. As stated above we are developing a new modified BRN2i that we will test in the one-year NCE.

Impact

- Loss of SWI/SNF complex subunits create dependencies and further loss of function within the same complex leads to synthetic lethality. Analogous to the BRN2/npBAF complex, disruption of the Myc/cBAF complex through inhibition of MAX and SMARCA4 is synthetically lethal in small cell lung cancer.
- Our BRN2 inhibitors combined with the recent discovery of BAF complex inhibitors including degraders like ACBl1 creates unique opportunity to explore the concept of synthetic lethality combining both BRN2 and BAF inhibition in NEPC.

Changes and problems

First, we would like to thank the DOD for the one-year extension for the period of September 1st 2021 through August 31st 2022 without any additional funding. Here the major reasons for a one-year extension.

- As highlighted by Dr. Corey and Dr. Morrissey that we encountered challenges with the in vivo study with lack of activity.
- Due to this, we requested a new synthesis of the drug; however, due to the COVID19 restriction, the synthesis of the drug was stalled and back ordered. For this reason, we couldn't get serum to perform aim 3 of the proposed project.
- Due to CIVID restriction UBC laboratories were closed until end of June 2020 and we still have restriction access with only 30% capacity and not allowed to work yet in the evenings; and similar restrictions were in place at the University of Washington.

These events impacted the timeline for all three investigators on this project. The one-year no-cost extension will allow us to complete both the animal studies and perform the downstream analysis as described in the application SOW at the University of Washington under IACUC protocol #3202-01, and use the serum to validate IGF-BP2/5 as a surrogate marker for BRN2i.

Another problem we are currently facing is the antibody that we used to develop the ELISA assay. This antibody is not working well and we don't have the same sensitivity. We are currently testing other antibodies for IGFBP5 ELISA. Moreover, we are looking to other approaches to allow us measure this marker in serum.

Participants

Dr. Amina Zoubeidi: University of British Columbia
Dr. Colm Morrissey: University of Washington
Dr. Eva Corey: University of Washington

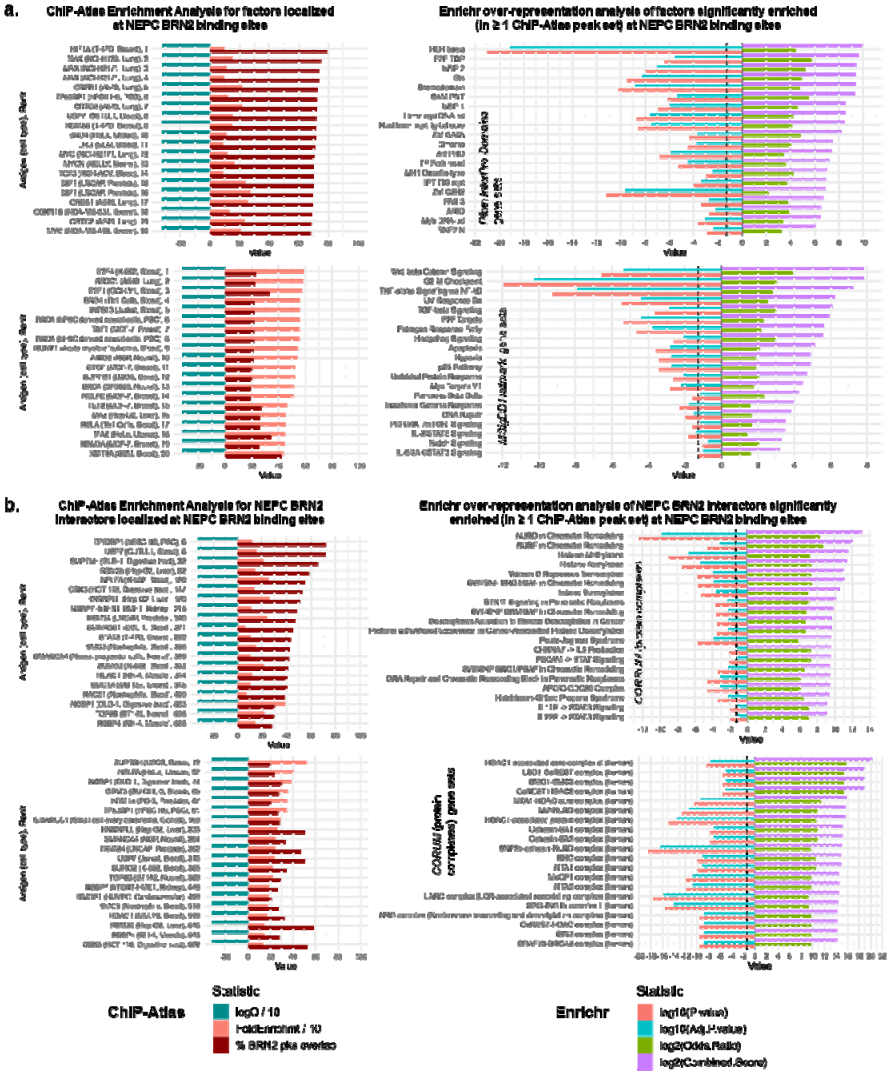

Figure 1. **(a)** ChIP-Atlas Enrichment Analysis results (left) for NEPC BRN2 Peak Set #2 and Enrichr analysis (right) for gene sets enriched among the most significant factors in the ChIP-Atlas results. ChIP-Atlas bar charts show the following three statistics for peak sets representing peaks called by MACS2 at log10Q < -10 for individual ChIP-seq experiments in the ChIP-Atlas database: log10 Q value divided by 10 ("logQ / 10") for the significance of their overlap with NEPC BRN2 peaks; the fold enrichment, divided by 10, of their overlap with NEPC BRN2 peaks relative to their overlap with random peaks ("FoldEnrichmt / 10"); and the percentage of NEPC BRN2 peaks that they overlap ("% BRN2 pks overlap"). ChIP-Atlas hits were ranked primarily by logQ and secondarily by either % overlap of BRN2 peaks (top left) or fold enrichment vs random (bottom left). The top 20 hits are shown (all shown hits had logQ = -324, the lowest calculable by ChIP-Atlas). Enrichr analysis was performed for the list of antigens having ≥ 1 ChIP-Atlas peak set satisfying logQ < -100, fold enrichment vs random > 10, and overlaps > 10% of NEPC BRN2 peaks in the ChIP-Atlas Enrichment Analysis results. Enrichr bar charts show four statistics calculated by Enrichr, for each gene set: log10(p value), where p is calculated by Fisher's exact test; log10 of the p value adjusted by the Benjamini-Hochberg method for the number of gene sets in a library; log2(odds ratio); and log2(combined score), where the combined score is the product of ln(p) and a z-score that assesses deviation from a pre-computed expected rank based on random gene sets. For each indicated gene-set library, the top 20 gene sets ranked by the combined score are shown in the bar charts. Vertical dashed line shows the threshold for $p < 0.05$. **(b)** Same as (a) but for just the antigens that were pulled down by IP for BRN2 but not IgG in ≥ 2/3 RIME experiments in 42D cells and 2/2 in NCI-H660 cells. Only the top ChIP-Atlas hit for each distinct antigen is shown in (b). Rank numbers correspond to the ranks of the ChIP-Atlas hits in the full ChIP-Atlas analysis from (a).

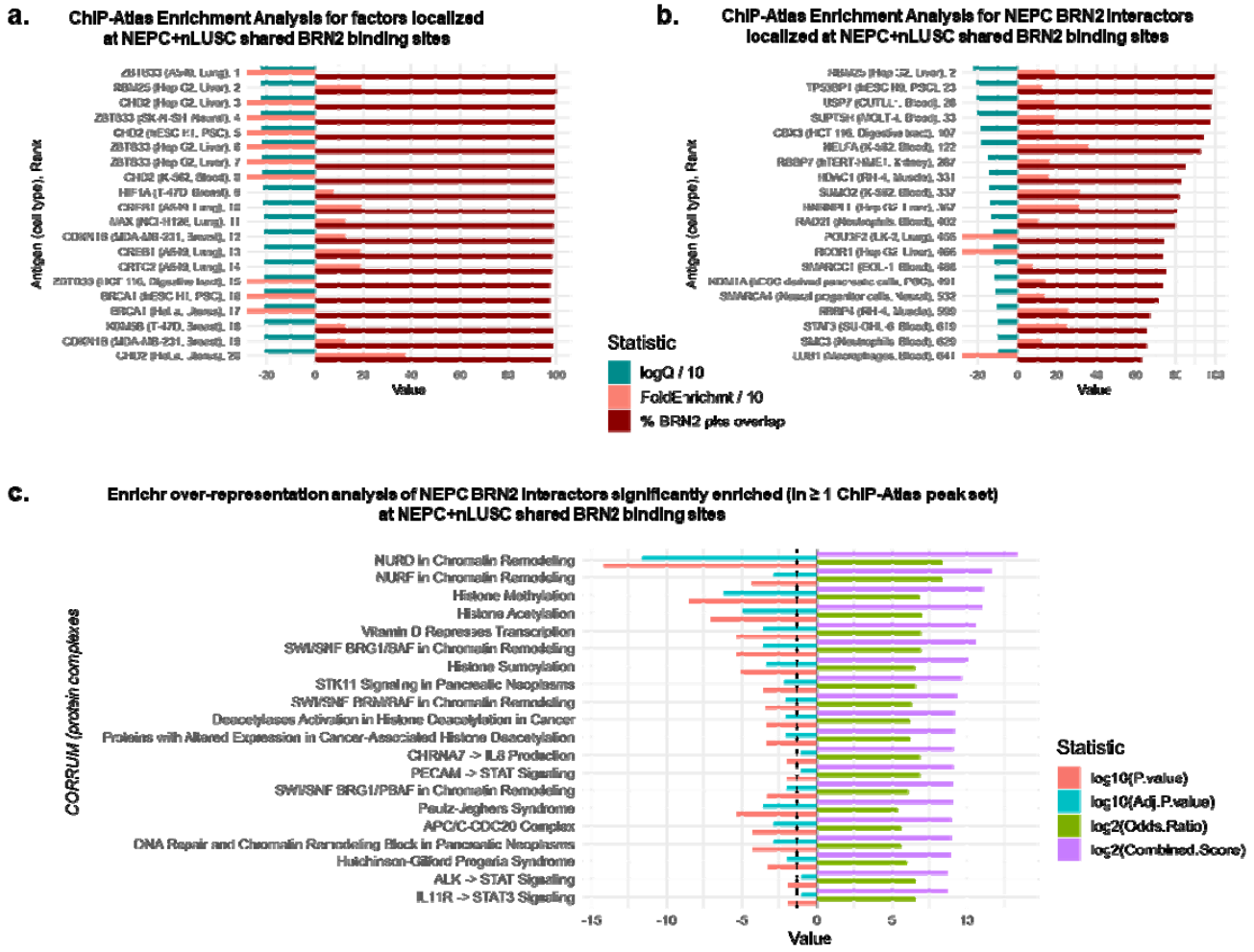

Figure 2. (a) ChIP-Atlas Enrichment Analysis results for the core set of 384 BRN2 peaks shared between NEPC and neural LUSC (nLUSC). ChIP-Atlas bar charts show the following three statistics for peak sets representing peaks called by MACS2 at log10Q < -10 for individual ChIP-seq experiments in the ChIP-Atlas database: log10 Q value divided by 10 ("logQ / 10") for the significance of their overlap with BRN2 peaks; the fold enrichment, divided by 10, of their overlap with BRN2 peaks relative to their overlap with random peaks ("FoldEnrichmt / 10"); and the percentage of BRN2 peaks that they overlap ("% BRN2 pks overlap"). ChIP-Atlas hits were ranked primarily by logQ and secondarily by % overlap of BRN2 peaks. A negative fold enrichment value is used to indicate that the fold enrichment was actually infinite because there were zero overlaps with random peaks**. (b)** Same as (a) but for just the antigens that were pulled down by IP for BRN2 but not IgG in ≥ 2/3 RIME experiments in 42D cells and 2/2 in NCI-H660 cells. Only the top ChIP-Atlas hit for each distinct antigen is shown in (b). Rank numbers correspond to the ranks of the ChIP-Atlas hits in the full ChIP-Atlas analysis from (a). **(c)** Enrichr analysis for overrepresentation of gene sets from the "Reactome 2016" library in the list of antigens having ≥ 1 ChIP-Atlas peak set satisfying logQ < -10, fold enrichment vs random > 10, and overlaps > 5% of BRN2 peaks in the ChIP-Atlas Enrichment Analysis results from (b). Bar charts show four statistics calculated by Enrichr, or transformations thereof, for each gene set: log10(p value), where p is calculated by Fisher's exact test; log10 of the p value adjusted by the Benjamini-Hochberg method for the number of gene sets in a library; log2(odds ratio); and log2(combined score), where the combined score is the product of ln(p) and a z-score that assesses deviation from a pre-computed expected rank based on random gene sets. The top 20 gene sets ranked by the combined score are shown. Vertical dashed line shows the threshold for $p < 0.05$.

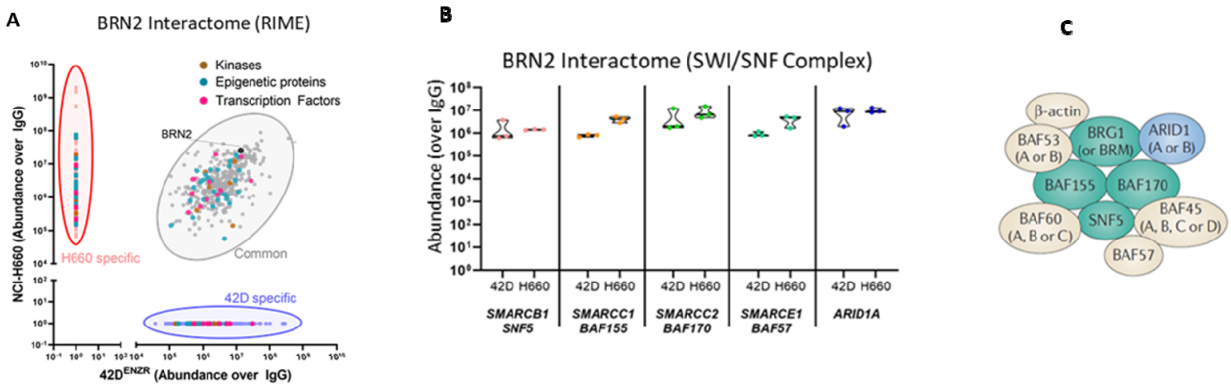

Figure 3: BRN2 interacts with SWI/SNF complex. **A)** Rapid immunoprecipitation mass spectrometry was performed in 42ENZR and NCI-H660 cells using BRN2 antibody and is presented by peptide abundance over IgG, common interactome in both cell lines. **B)** SWI/SNF core member peptide abundance in 42DENZR and NCI. **C)** cartoon showing SWI/SNF complex.

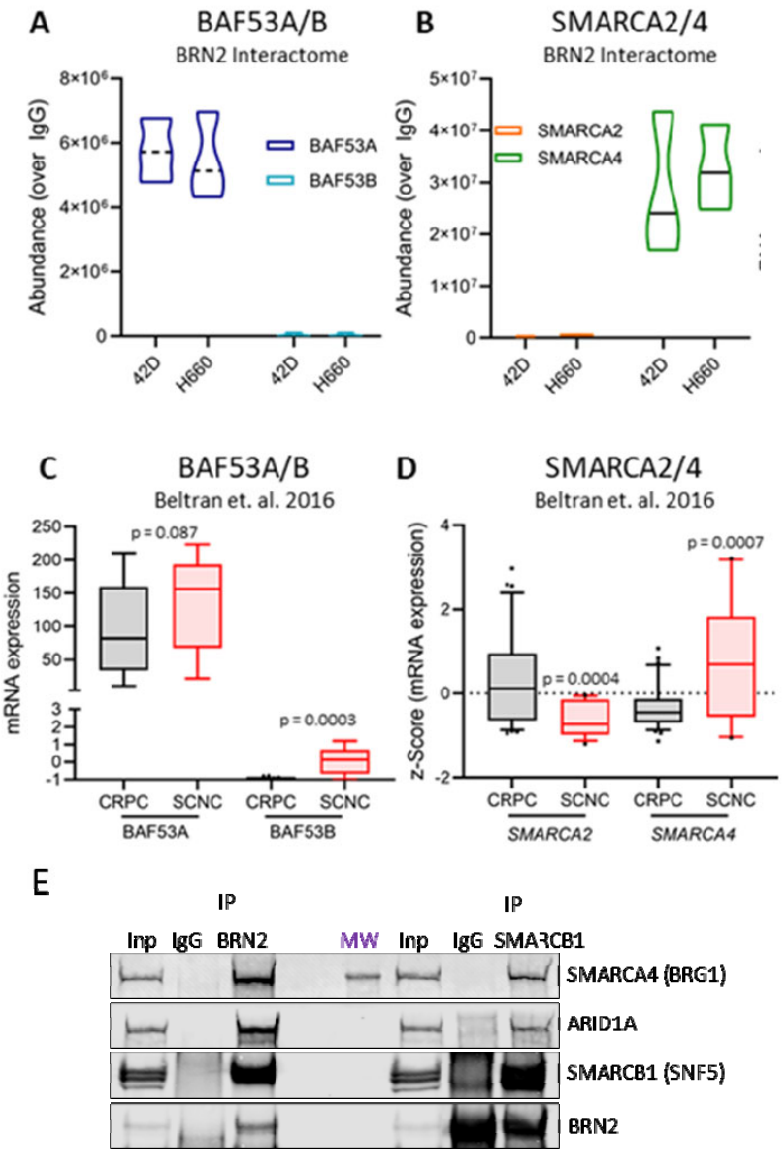

Figure 4: BRN2 interacts preferentially with BAF53B (**A)** and SMARCA4 **(B)** as shown by peptide abundance. Expression of BAF53A and BAF53B **(C)** and SMARCA2 and SMARCA4 **(D)** in CRPC and NEPC patients from Beltran dataset. **E)** Total extract from 42DENZR cells was immunoprecipitated with BRN2 or SMARCAB1 with IgGs, western blots were performed with SMARCA4, ARID1A, SMARCB1 and BRN2 to show the interaction between BRN2 and SWI/NNF complex.

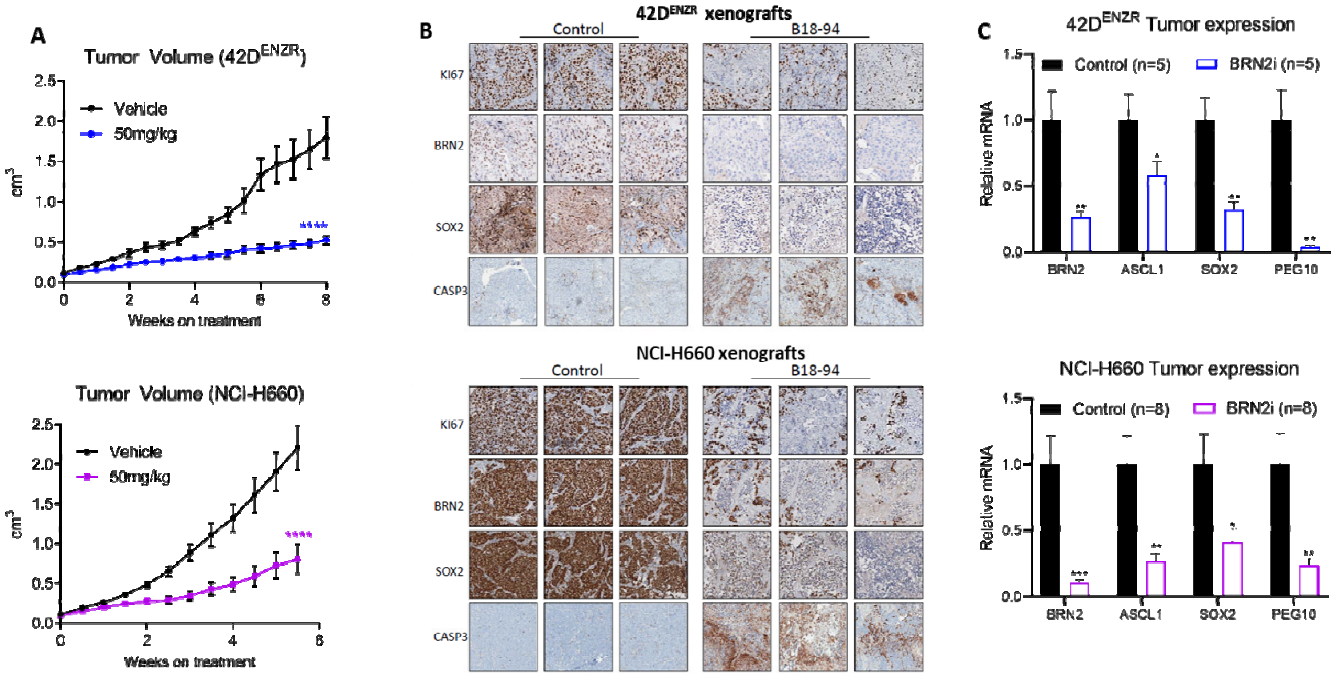

Figure 5: *In vivo* efficacy of BRN2 inhibitor: Xenograft of 42D^{ENZR} and NCI-H660 injected into Nu/Nu mice. Mice were treated with indicated doses of B18-94 when tumor volume reached 100mm^3. **(A)** Tumor volume of 42D^{ENZR} (upper panel) and NCI-H660 (lower panel) xenografts treated with control and 50mg/kg of B18-94. B) Immunohistochemistry from 3 representative tumors staining for BRN2, SOX2, Ki67 and CASP3 in 42D^{ENZR} (upper panel) and NCI-H660 (lower panel). Average expression of BRN2 target genes from different tumors as measured by qRT-PCR for indicated target genes in different tumors in 42D^{ENZR} (upper panel) and NCI-H660 (lower panel).

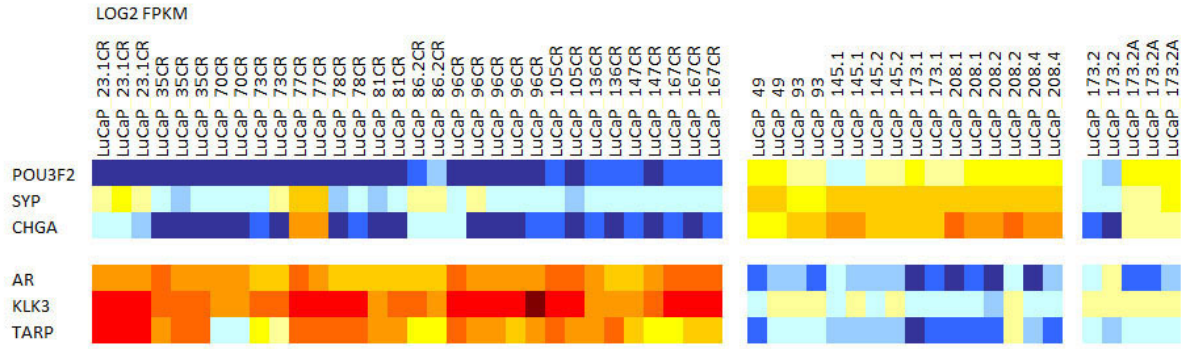

Figure 6. BRN2 expression by RNAseq in LuCaP PDX models. LuCaP 173.2 is an early passage, LuCaP 173.2A is a later passage.

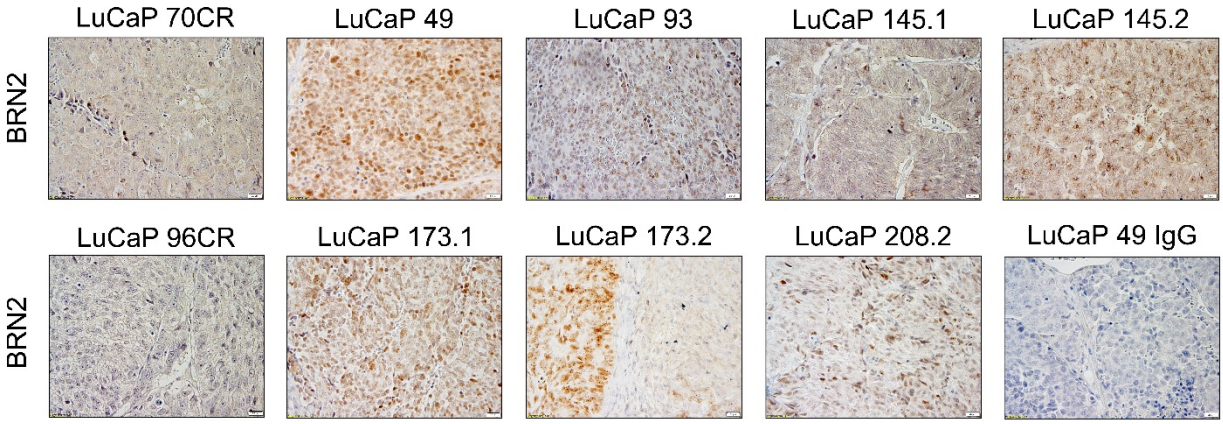

Figure 7. BRN2 localization in LuCaP PDX models. Immunohistochemistry of LuCaP 70CR and 96CR (adenocarcinoma) and LuCaP 49, 93, 145.1, 145.2, 173.1, and 208.2 (neuroendocrine), and LuCaP 173.2 (mixed neuroendocrine and double-negative) LuCaP PDX models. Including IgG control.

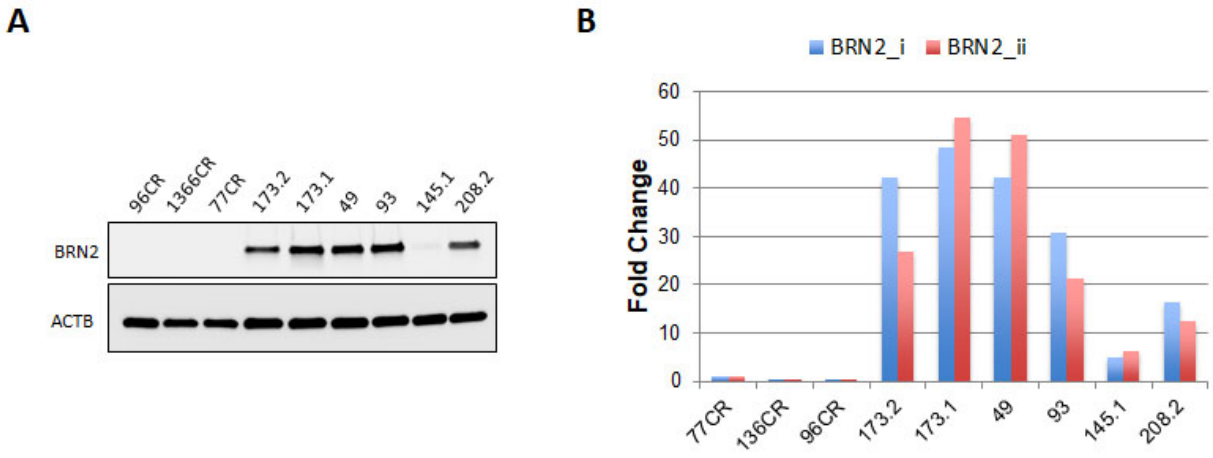

Figure 8. BRN2 expression in LuCaP PDX models. (A) Immunoblot analyses of tumor lysates from LuCaP PDX models (n=9). (**B**) qPCR of LuCaP PDX tumors. Fold changes of BRN2_i (primer set 1) and BRN2_ii (primer set 2) are displayed and expression was normalized to constitutively active ACTB gene expression and relative to LuCaP 77CR.

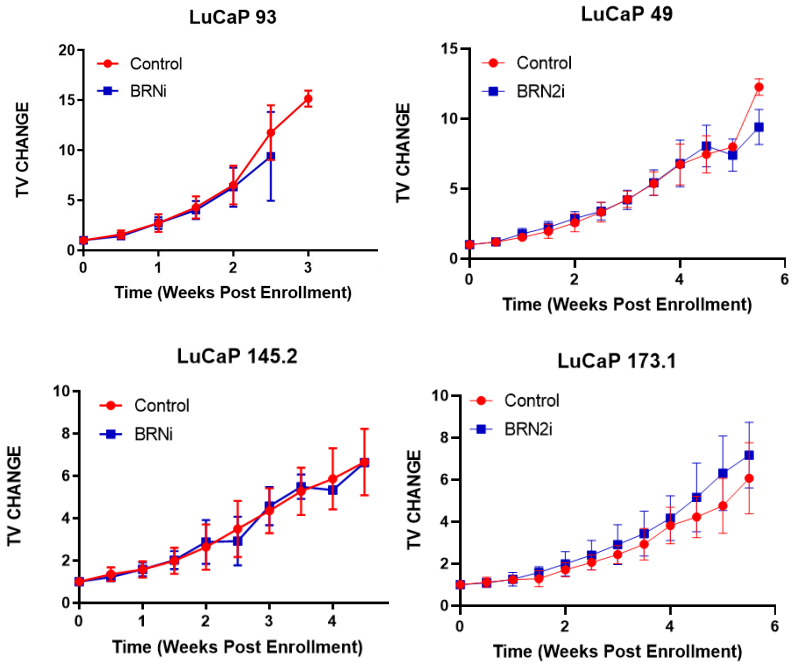

Figure 9. Change in normalized tumor volume (TV) after BRN2i treatment in LuCaP 93, 49, 145.2 and 173.1. No significant differences in tumor volume were observed in any of the patient-derived xenograft lines after treatment with the BRN2i.

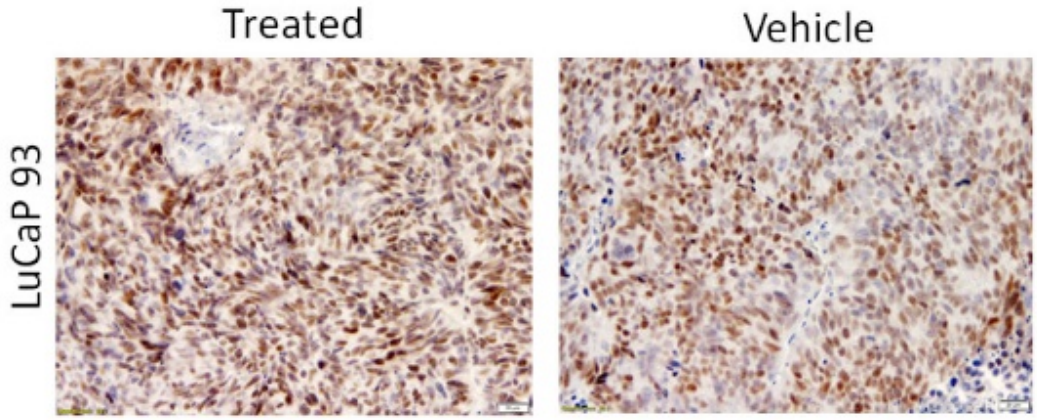

Figure 10. BRN2 expression in LuCaP 93. An example of BRN2 staining by immunohistochemistry in BRN2i treated and vehicle treated LuCaP 93 PDX tumors.

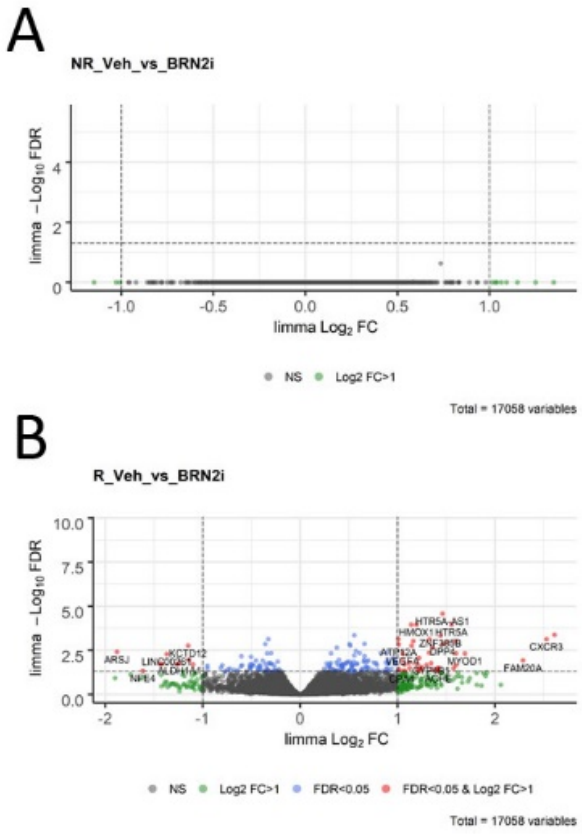

Figure 11. Volcano plots of genes differential expressed in vehicle control versus BRN2i treated tumors. BRN2 positive non-responsive LuCaP xenografts LuCaP 49, 93 and 173.1 (A) did not display any significant changes in gene expression relative to the BRN2i responsive NCIH660 and enzalutamide resistant 42D cells (B).

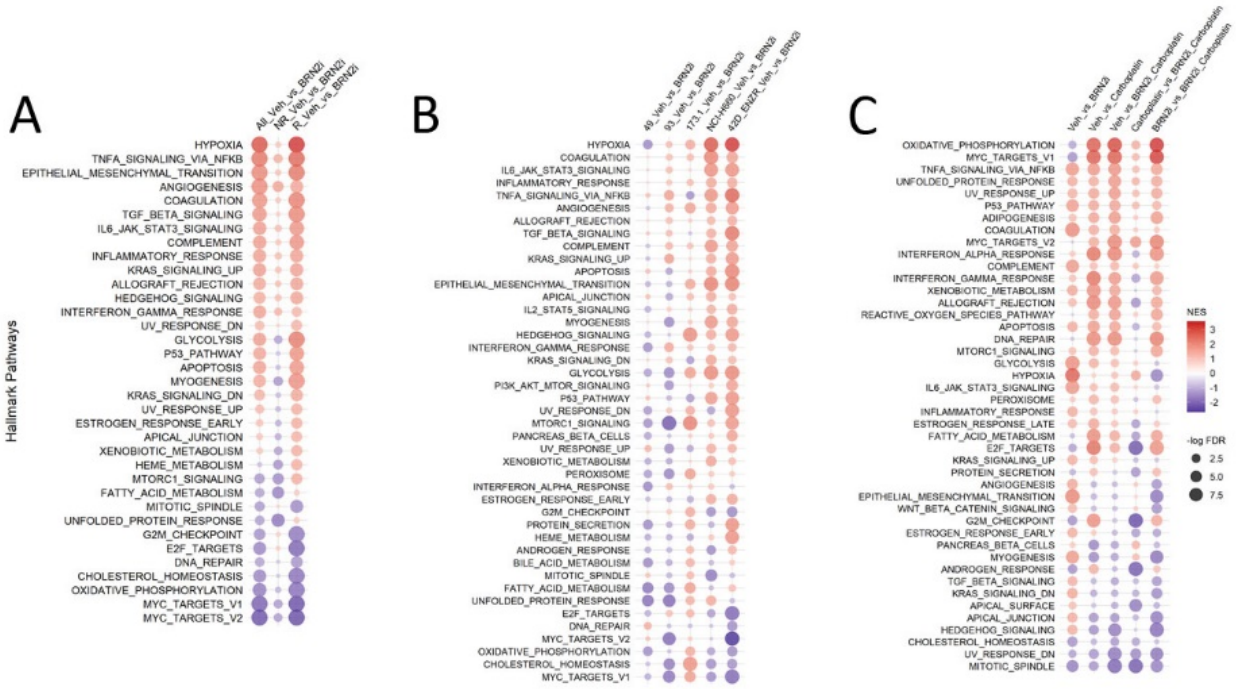

Figure 12. Hallmark Pathways switched on in BRN2 responsive and Carboplatin responsive tumors. Hallmark pathway comparing all, non-responsive and responsive BRN2i treated tumors (A), each line individually (B), and response to BRN2i and carboplatin as a monotherapy and as a combination therapy.

References

CUELLA-MARTIN, R., OLIVEIRA, C., LOCKSTONE, H. E., SNELLENBERG, S., GROLMUSOVA, N. & CHAPMAN, J. R. 2016. 53BP1 Integrates DNA Repair and p53-Dependent Cell Fate Decisions via Distinct Mechanisms. *Mol Cell,* 64**,** 51-64.

KIM, H. & YIM, H. 2018. 53BP1: A guardian for centrosomal integrity. *Front Biosci (Landmark Ed),* 23**,** 1-12.

LUO, J., SU, F., CHEN, D., SHILOH, A. & GU, W. 2000. Deacetylation of p53 modulates its effect on cell growth and apoptosis. *Nature,* 408**,** 377-81.

SCHULTZ, L. B., CHEHAB, N. H., MALIKZAY, A. & HALAZONETIS, T. D. 2000. p53 binding protein 1 (53BP1) is an early participant in the cellular response to DNA double-strand breaks. *J Cell Biol,* 151**,** 1381-90.

SMEENK, G., WIEGANT, W. W., VROLIJK, H., SOLARI, A. P., PASTINK, A. & VAN ATTIKUM, H. 2010. The NuRD chromatin-remodeling complex regulates signaling and repair of DNA damage. *J Cell Biol,* 190**,** 741-9.

YIM, H., SHIN, S. B., WOO, S. U., LEE, P. C. & ERIKSON, R. L. 2017. Plk1-mediated stabilization of 53BP1 through USP7 regulates centrosome positioning to maintain bipolarity. *Oncogene,* 36**,** 966-978.